J. Fluid Mech. (2007), *vol.* 573, *pp.* 237–246. © 2007 Cambridge University Press
doi:10.1017/S0022112006004174 Printed in the United Kingdom

A double-helix laminar dynamo

L. ZABIELSKI[1] AND A. J. MESTEL[2]

[1]Mathematics Department, Warsaw University of Technology, 00-661 Warsaw, Poland

[2]Mathematics Department, Imperial College London, SW7 2AZ, UK

(Received 5 September 2006 and in revised form 22 November 2006)

It has recently been shown that laminar, pressure-driven flow of a conducting fluid in a helical pipe can generate a dynamo. Geometrical constraints have hitherto required a relatively small Reynolds number, and a much larger magnetic Reynolds number, R_m. Here, a configuration with two interwoven helical pipes is considered which is shown to drive a dynamo at a Reynolds number of a few hundred and $R_m > 30$. Various computer animations of the dynamo are available with the online version of the paper. It is found that hydrodynamic instabilities may inhibit the dynamo, but may also be regularized by it. It is also shown that a dynamo pump is possible, with flow down one pipe generating a field which drives flow in the second. Movies are available with the online version of the paper.

1. Introduction

The ability of motion of a conducting fluid to generate and sustain a magnetic field is important in astrophysical and geophysical contexts. On such length scales, not only is the motion likely to have a complex turbulent structure, but also the magnetic Reynolds number, R_m, is very high. Such dynamos typically rely on a turbulent 'α-effect,' wherein averages over small-scale fluctuations arguably lead to an extra mean field term in the driving equations, e.g. Roberts & Soward (1992). A recent introduction to the problem is given by Gilbert (2003). Dynamos on engineering scales are also possible, and have been built in Riga and Karlsrühe as in Rädler & Cēbers (2002). This paper investigates a geometry similar to the Karlsrühe dynamo, which used fluted pipes to drive helical motion, which is considered advantageous for dynamo action.

Recently, Zabielski & Mestel (2006) showed that laminar, pressure-driven flow in a helical pipe is capable of sustaining dynamo action. For suitable pipe geometry, there is a narrow range of hydrodynamic Reynolds number R_e for which magnetic growth appears. The critical value of the magnetic Reynolds number R_m for these flows was about 10^3. R_e had to be chosen so that the cross-pipe (secondary) flow consisted of two circulating regions, one of which was too weak to destroy the dynamo. This constraint only permitted dynamos at high magnetic Prandtl number, R_m/R_e. As a result, the dynamo was viscously dominated. Strong magnetic fields were created and destroyed by the fluid motion with the nonlinear behaviour only weakly dependent on Ohmic dissipation. The fields exhibited reversals, and were occasionally totally quenched, before re-establishing themselves on a slow time scale. The calculations assumed perfectly conducting walls, although similar behaviour was found with lower external conductivity.

The single-pipe helical dynamo only exists for high R_m in a narrow range of R_e. In this paper an interwoven, two-pipe configuration is considered in which one

https://doi.org/10.1017/S0022112006004174 Published online by Cambridge University Press

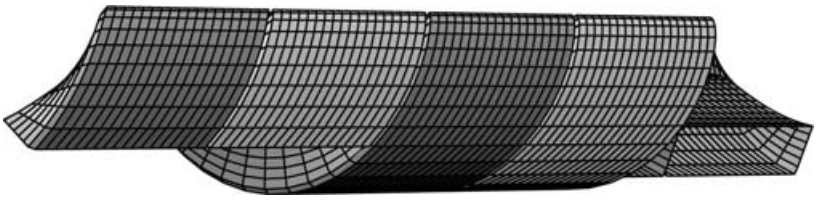


FIGURE 1. The two-pipe system with z-axis to the left. Flow in each pipe is in opposite sense.

rectangular helical pipe alternates with another. The two pipes fit together so that they exactly fill a cylindrical annulus as shown in figure 1. The flow passes down one pipe and returns through the other. Significantly, the pipes are in electrical contact, so that current can pass from one to the other. It is found that this configuration drives a dynamo at higher R_e and lower R_m, with kinematic growth rates larger by a factor of 10.

The problem is formulated in § 2. The steady flow through the two-pipe system is antisymmetric about the helical interface between the pipes. Solutions for the magnetic field may be symmetric or antisymmetric (or neither). Calculation in § 3 shows that the preferred solutions are symmetric and this symmetry is closely preserved into the nonlinear regime. The region of (R_e, R_m) space for which dynamo action occurs is identified. Growth is found to occur for both $R_e > R_m$ and $R_e < R_m$.

In § 4, the dynamo behaviour is shown to vary considerably with R_e. For $R_e = 69$, the low critical value $R_m = 29.7$ is found. As R_m is increased above this value the field first equilibrates at a steady level before bifurcating to a periodic oscillation.† As R_m increases further the solution loses periodicity. An active phase is encountered, with comparable magnetic and kinetic energies. For larger R_m the high field energy cannot be maintained, and it reduces dramatically. The field is not found to reverse, in contrast to the cases considered in Zabielski & Mestel (2006).

At lower values of R_e, much higher magnetic energy levels are attained, often exceeding the kinetic energy. Furthermore, the magnetic energy appears to remain large at high R_m, even though the dynamo is 'slow.'†

At low to moderate values of R_e, calculation shows that there is a unique steady flow. However, at higher R_e, the driving flow is prone to a hydrodynamic instability of Görtler type on the outer wall. The resulting unsteady flow is less conducive to dynamo action, which then occurs only in a finite interval of R_m. When a dynamo does occur, it exerts a regularizing influence on the unsteady flow. The dynamo window shrinks and vanishes as R_e increases, so that a turbulent dynamo would require a different mechanism. The competition between hydrodynamic and dynamo instabilities is a new effect, as no other pressure-driven, laminar dynamo is known. It is also shown that flow down one pipe is capable of driving flow down a separate pipe by means of the induced dynamo action.

2. Formulation of the problem

Only helically symmetric fields are considered in this paper. While it is certainly possible that the dynamo would not exhibit the helical symmetry of the geometry, experience with the related Ponomarenko problem suggests the preferred dynamo mode will be nearly symmetric (Gailitis & Freiberg 1977). In terms of cylindrical polar coordinates (r, θ, z), a scalar function is helically symmetric if it depends only

† Animations of these cases are available with the online version of the paper.

https://doi.org/10.1017/S0022112006004174 Published online by Cambridge University Press

on r and $\phi = \theta + \varepsilon z$, where ε is a constant. To be single-valued, the function must also be 2π-periodic in ϕ and it is constant on helices with the same pitch, $2\pi/\varepsilon$. The symmetry direction is given by the vector

$$\boldsymbol{H} = (\boldsymbol{e}_z - \varepsilon r \boldsymbol{e}_\theta)/h^2 \qquad \text{where} \quad h = (1 + \varepsilon^2 r^2)^{1/2} \tag{2.1}$$

and $\boldsymbol{e}_\theta$ and $\boldsymbol{e}_z$ are the unit vectors in the θ- and z-directions. Thus a scalar field f is helically symmetric if $\boldsymbol{H} \cdot \nabla f = 0$. The vector $\boldsymbol{H}$ is a non-unit Beltrami field

$$\nabla \wedge \boldsymbol{H} = -2\varepsilon \boldsymbol{H}/h^2, \qquad |h\boldsymbol{H}| = 1. \tag{2.2}$$

A detailed description of helical symmetry is given in Zabielski & Mestel (1998). It spans the gulf between two-dimensionality ($\varepsilon = 0$) and axisymmetry ($\varepsilon \to \infty$). This paper concentrates on the case $\varepsilon = 1$ for the two rectangular pipes drawn in figure 1. The pipes interlock to fill the entire annulus $0.5 < r < 1.5$. The pipe boundaries are $\phi = 0, \pm\pi$.

The helically symmetric velocity, $\boldsymbol{u}$, and magnetic field, $\boldsymbol{B}$, are both solenoidal and are represented by two scalar functions

$$\boldsymbol{u} = \boldsymbol{H} \wedge \nabla\Psi + v\boldsymbol{H} \qquad \text{and} \qquad \boldsymbol{B} = \boldsymbol{H} \wedge \nabla\chi + B\boldsymbol{H}. \tag{2.3}$$

The corresponding vorticity $\omega = \nabla \wedge \boldsymbol{u}$ and current density $\boldsymbol{j} = \nabla \wedge \boldsymbol{B}$ then take the form

$$\omega = \boldsymbol{H} \wedge \nabla(-v) + \xi \boldsymbol{H}, \qquad \boldsymbol{j} = \boldsymbol{H} \wedge \nabla(-B) + \gamma \boldsymbol{H}, \tag{2.4}$$

where

$$\xi = \mathscr{L}\Psi - 2\varepsilon v/h^2 \qquad \text{and} \qquad \gamma = \mathscr{L}\chi - 2\varepsilon B/h^2, \tag{2.5}$$

with the elliptic operator $\mathscr{L}$ defined by $\mathscr{L} \equiv h^2 \nabla \cdot (h^{-2}\nabla)$. Suitably non-dimensionalized, $\boldsymbol{u}$ and $\boldsymbol{B}$ satisfy the Navier–Stokes equations

$$\frac{\partial \boldsymbol{u}}{\partial t} + \boldsymbol{u} \cdot \nabla \boldsymbol{u} = -\nabla p + \boldsymbol{j} \wedge \boldsymbol{B} + R_e^{-1} \nabla^2 \boldsymbol{u}, \qquad \nabla \cdot \boldsymbol{u} = 0 \tag{2.6}$$

and the magnetic induction equation

$$\frac{\partial \boldsymbol{B}}{\partial t} = \nabla \wedge (\boldsymbol{u} \wedge \boldsymbol{B}) + R_m^{-1} \nabla^2 \boldsymbol{B}, \qquad \nabla \cdot \boldsymbol{B} = 0, \tag{2.7}$$

where R_e and R_m are the hydrodynamic and magnetic Reynolds numbers, for non-dimensionalization with respect to the driving pressure gradient and the pipe width. The imposed pressure gradient is alternately up and down the pipes, so that the pressure itself is not helically symmetric, but can be written in the non-dimensional form

$$p = \mp z + \widehat{p}(r, \phi) \tag{2.8}$$

with a sign appropriate to the flow direction in the two pipes. The components of equations (2.6)–(2.7) are given in Zabielski & Mestel (2005). A similar magnetic field representation was derived by Lortz (1968) and Benton (1979). In component form, it is readily seen that the equations for B and χ, which are respectively the helical analogues of toroidal and poloidal fields, are linked because of the Beltrami property (2.2) of the helical symmetry direction $\boldsymbol{H}$. It is this 'geometrical α-effect' which permits a laminar helical dynamo, which by Cowling's theorem is not possible in the axisymmetric ($\varepsilon \to \infty$) and the two-dimensional ($\varepsilon = 0$) limits.

Equations (2.6) and (2.7) determine the time evolution of the velocity and magnetic fields. On the rigid pipe boundaries the velocity satisfies

$$\boldsymbol{u} = 0 \qquad \text{on } r = 0.5,\ 1.5, \qquad \phi = 0,\ \pm\pi. \tag{2.9}$$

https://doi.org/10.1017/S0022112006004174 Published online by Cambridge University Press

Perfectly conducting walls are assumed at $r = 0.5$ and $r = 1.5$, so that

$$\chi = 0, \qquad \frac{\partial B}{\partial r} = 0 \qquad \text{on } r = 0.5,\ 1.5. \tag{2.10}$$

The interfaces between the pipes at $\phi = 0,\ \pi$ are assumed to have the same conductivity as the fluid so that χ and B vary smoothly in the ϕ-direction. The magnetic boundary conditions are then 2π-periodicity in ϕ. Below, it is found that the field exhibits symmetry about the ϕ-boundaries, in which case the periodicity constraints may be replaced by the Neumann conditions

$$\frac{\partial B}{\partial \phi} = 0, \qquad \frac{\partial \chi}{\partial \phi} = 0 \qquad \text{on } \phi = 0,\ \pi. \tag{2.11}$$

A discussion of other magnetic boundary conditions is given in Zabielski & Mestel (2005).

3. Numerical solutions

The Navier–Stokes and induction equations (2.6) and (2.7) are invariant with respect to helical symmetry, and only helically symmetric solutions will be considered. In addition, the equations are invariant with respect to the transformation

$$\phi \to -\phi, \quad v \to -v, \quad \Psi \to -\Psi, \quad \boldsymbol{H}\cdot\nabla p \to -\boldsymbol{H}\cdot\nabla p. \tag{3.1}$$

As the pipe cross-section is symmetric with respect to ϕ, it follows that reversing the direction of the pressure gradient merely inverts the top and bottom of the pipe. Thus the steady flow driven up one pipe and down the other has symmetry about the pipe boundary $\phi = 0$. It should be noted that this symmetry does not reverse all velocity components: the down-pipe flow (v) is reversed, but the cross-pipe flow is symmetric in ϕ. The magnetic field may exhibit the same symmetry; equally, as the Lorentz force $\boldsymbol{j} \wedge \boldsymbol{B}$ is quadratic it could be antisymmetric without disturbing the flow symmetry. Thus as the system evolves in time there will be a solution for which both $\boldsymbol{u}$ and $\boldsymbol{B}$ are symmetric about $\phi = 0$ in the above sense and one where $\boldsymbol{u}$ is symmetric and $\boldsymbol{B}$ is antisymmetric. The former case can be represented by solution over the reduced domain $0 < \phi < \pi$ with the Neumann conditions (2.11), and the latter by the Dirichlet conditions of vanishing χ and B. It is found that the system prefers the symmetric state.

Equations (2.6) and (2.7) are solved numerically using second-order, implicit time-stepping with centred spatial differences as described in Zabielski & Mestel (2006). The grid size is $1/200$ in the r-direction and $\pi/600$ in the ϕ-direction. For $R_e = 69$ the steady flow is shown in figure 2(a–c). The maximum value of v is about 5 in this case, so that the effective Reynolds number is arguably a few hundred. Figures 1(a), 1(b) and 1(c) depict contours of Ψ, v and ξ. The inside of the pipe is on the left and the pipe climbs up out of the page. The flow structure, with two secondary vortices and nearly vertical v-contours resembles Dean flow at high Dean number (Berger, Talbot & Yao 1983). As R_e is increased (with no magnetic field), the steady flow becomes unstable. Disturbances appear in the boundary layer on the outer wall which at high R_e intermittently erupt out of the layer. This instability of a boundary layer on a curved wall is thought to be of Görtler type, as described by Hall & Horseman (1991). The resulting unsteady flow is found to be less conducive to dynamo action, but need not extinguish it.

https://doi.org/10.1017/S0022112006004174 Published online by Cambridge University Press

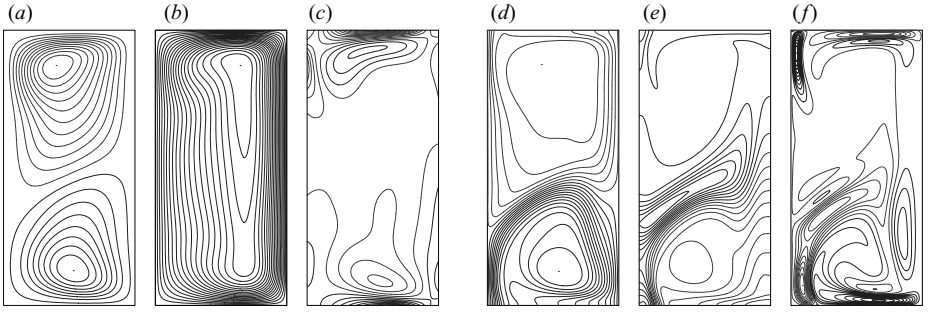


FIGURE 2. Steady flow in each pipe for $R_e = 69$ and the linearly growing magnetic field for $R_m = 512$. $(a–f)$ $\Psi, v, \xi, \chi, B, \gamma$. The inside of the helix is on the left, with r horizontal and ϕ vertical. Note the strong dependence of the field on the shape of Ψ.

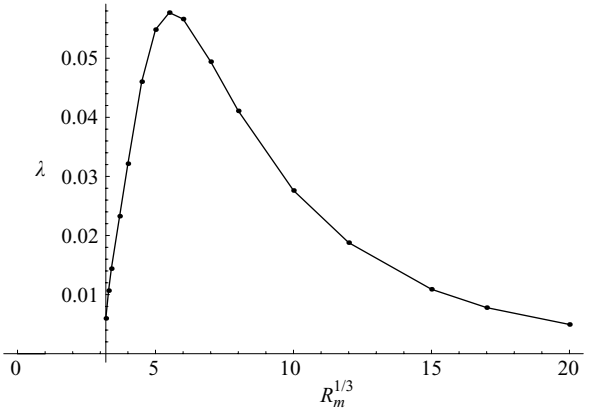


FIGURE 3. The linear growth rate as a function of R_m for the flow of figure 2.

For the flow of figure 2, a dynamo is found for $R_m > 30$. Both the symmetric and antisymmetric modes have positive growth rates, but the symmetric growth rate is higher for all R_m and so is preferred in the time evolution. The kinematic eigenfunction is drawn on figure $2(d–f)$ for $R_m = 8^3$. The growing field is heavily influenced by the shape of Ψ, especially for large R_m. The linear growth rate, λ, is plotted against $R_m^{1/3}$ in figure 3. This is a 'slow' dynamo, since $\lambda \to 0$ as $R_m \to \infty$. In fact $\lambda \sim R_m^{-1/3}$ as $R_m \to \infty$, and so the one-third power is an appropriate scaling for R_m.

It might be expected that symmetry would be broken during the nonlinear evolution. However, numerical solution of the full nonlinear problem over the double-pipe domain shows that the variation from symmetry is very small, certainly less than 1%, for all cases where the symmetric solution is either steady or time-periodic. A similar result holds when the magnetic energy remains small. The main reason for this is the no-slip condition satisfied by the velocity on $\phi = 0$. Although symmetry is not imposed, this condition severely restricts the possible flow behaviour, and the combined system prefers to remain almost symmetric.

When the symmetric solution exhibits chaotic time behaviour, however, the situation is different. The occasional departures from symmetry, which are observed near energy peaks, soon lead to large divergence between the symmetric and non-symmetric solutions. Even though the variations from symmetry remain small for all time, the

https://doi.org/10.1017/S0022112006004174 Published online by Cambridge University Press

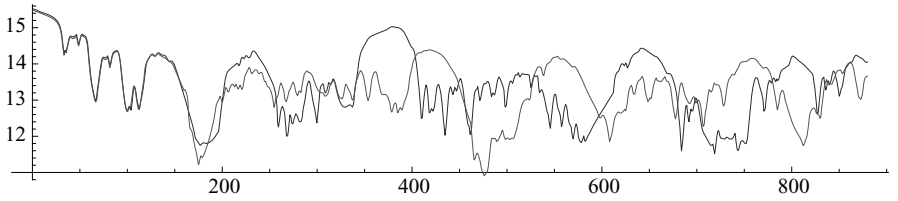


FIGURE 4. Variation between the solutions with and without imposed symmetry for $R_e = 69$ and $R_m = 512$. The chaotic time behaviour ensures that small divergences have long term effect. The darker line is the symmetric solution.

divergence between solutions becomes marked, as can be seen from the energy traces in figure 4.

From now on, both the velocity and field are constrained to be symmetric, as suggested by the linear solution. The dynamo is allowed to evolve dynamically in figures 5 and 6 for various values of R_m. Both the kinetic energy $E_k(t)$ and the magnetic energy $E_m(t)$ are shown, defined for a suitable pipe section V by

$$2E_k(t) = \int_V \boldsymbol{u}\cdot\boldsymbol{u}\,\mathrm{d}V, \qquad 2E_m(t) = \int_V \boldsymbol{B}\cdot\boldsymbol{B}\,\mathrm{d}V. \tag{3.2}$$

For slightly supercritical R_m, the dynamo saturates in a steady state, with $E_m \ll E_k$. As R_m increases, E_m/E_k at first increases. A periodic oscillation sets in at about $R_m = 57$, and continues past $R_m = 125$. A detailed animation of this oscillation is available with the online version of the paper (animation 1). The negative contours of $\boldsymbol{u}\cdot\boldsymbol{j}\wedge\boldsymbol{B}$ illustrated in the animation indicate that the magnetic energy is generated near the stagnation point of Ψ on the inner wall. The oscillation period is close to the turnover time of the cross-pipe vortices. Intermittently, structures appear on the outer wall which resemble the hydrodynamic instability found at higher R_e.

As R_m continues to increase the periodicity is lost. The mean of E_m increases steadily until a sudden transition to a solution with low magnetic energy occurs. For $3242 \geqslant R_m \geqslant 12^3$, self-quenching, high-energy solutions are found, with the field almost disappearing intermittently, before re-establishing itself on the kinematic time scale. The quenching is perhaps a precursor to loss of stability in the high-energy solution, since for $R_m \geqslant 3375$, only low-energy solutions are found, as shown in figure 6. The flow is only slightly disturbed from the steady state, and an almost periodic solution is recovered for high R_m. The oscillation mechanism differs from that of lower R_m in that it involves structures being shed from a thin layer along the separation line of Ψ rather than the behaviour on the outer wall.

4. Variation with R_e

Dynamos are found in a range of hydrodynamic Reynolds number, $R_e^{min} < R_e < R_e^{max}$. Here R_e^{min} is governed by the shape of the flow, in particular by the structure of the cross-pipe component, Ψ. No dynamo action is found when Ψ consists of a single circulatory region, as occurs at low R_e (Zabielski & Mestel 1998). It is believed that R_e^{min} corresponds to the creation of a sizable second region, and that (weak) dynamo action then occurs at very high R_m. The upper limit R_e^{max} is related to hydrodynamic instability.

As R_e increases from R_e^{min} up to a value $R_e = R_0$, a critical value R_m^c is found such that a dynamo occurs in the semi-infinite range $R_m > R_m^c$. For $R_e > R_0$, the

https://doi.org/10.1017/S0022112006004174 Published online by Cambridge University Press

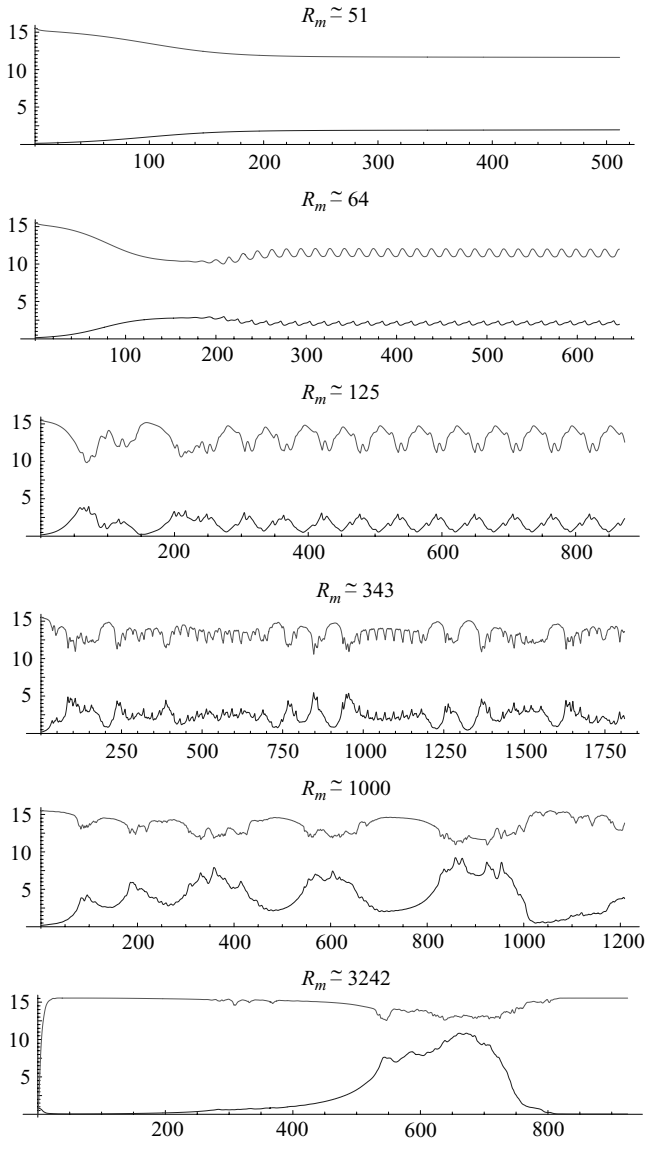


FIGURE 5. Energy traces $E_k(t)$ (top) and $E_m(t)$ (bottom) for $R_e = 69$ and various R_m.

steady pipe flow is unstable. This instability first appears on the outer wall and saturates as a periodic oscillation. While this oscillation has small amplitude it does not prevent dynamo action for moderate R_m values. Indeed, R_m^c is slightly lower for the time-periodic flow at $R_e = 83.5$ than for the steady flow at $R_e = 69$. However, for large R_m, for which any growth rate would be small, even a weak hydrodynamic oscillation is found to inhibit the dynamo. Thus for R_e slightly greater than R_0, there is a finite window of dynamo action $R_m^c < R_m < R_m^{max}$. As R_e increases further, the time-dependent part of the flow grows in magnitude and the dynamo window shrinks, disappearing to a point at $R_e = R_e^{max}$, as shown in figure 7. If a dynamo does occur for an unsteady flow it exerts a regularizing influence on the velocity. In figure 8 the chaotic flow for $R_e \simeq 91$ is rendered periodic by the dynamo.

https://doi.org/10.1017/S0022112006004174 Published online by Cambridge University Press

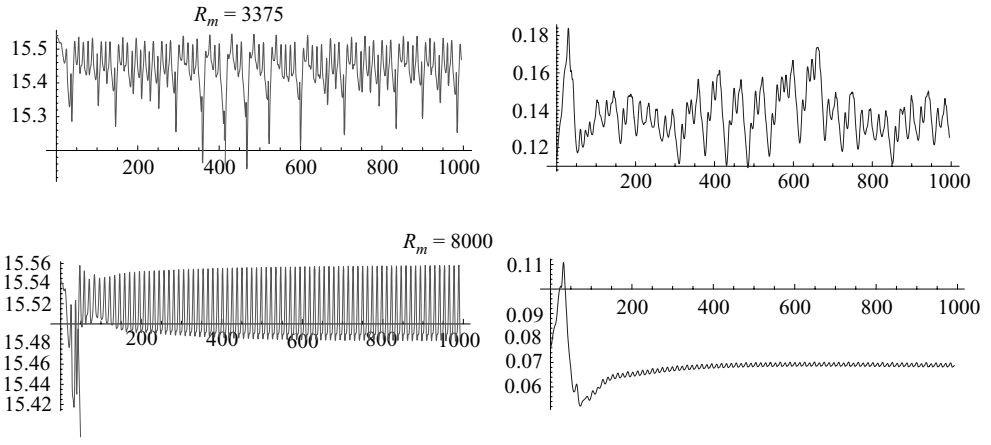


FIGURE 6. $E_k(t)$ (left) and $E_m(t)$ (right) for $R_e = 69$ and $R_m = 15^3,\ 20^3$. Here $E_k \gg E_m$.

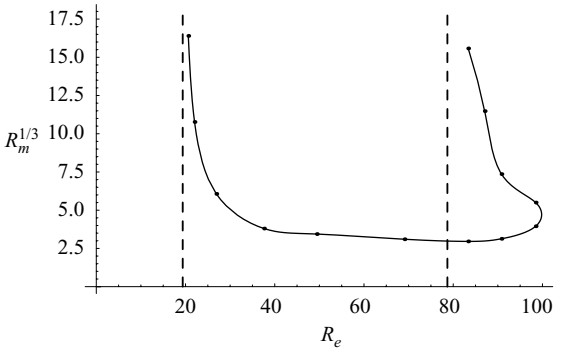


FIGURE 7. The region of dynamo action is above the curve. The rightmost vertical dashed line indicates the transition to unsteady driving flow. The unsteady flow can support a dynamo. The left asymptote corresponds to where Ψ develops a discernible second vortex.

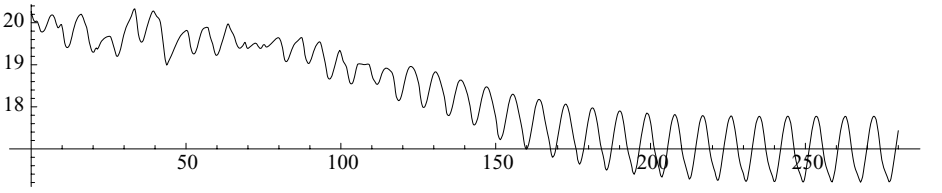


FIGURE 8. $E_k(t)$ for $R_e = 91$ and $R_m \simeq 39$. The aperiodic flow is regularized by the dynamo.

It should not be forgotten that once the flow ceases to be steady there is some indeterminacy in the problem. The flows in the two pipes are essentially time-periodic, but the phase difference between these independent flows is arbitrary, determined by noise in the initial condition. While the amplitude of the oscillation remains small, this has only limited effect on the field generation and the field is almost symmetrical. Indeed, the presence of the dynamo probably leads to phase locking between the two periodic pipe flows, but this has not been investigated.

For high R_e, the hydrodynamic instability, which is of Görtler type, being essentially that of a boundary layer on a concave wall, appears to kill the dynamo. This is

https://doi.org/10.1017/S0022112006004174 Published online by Cambridge University Press

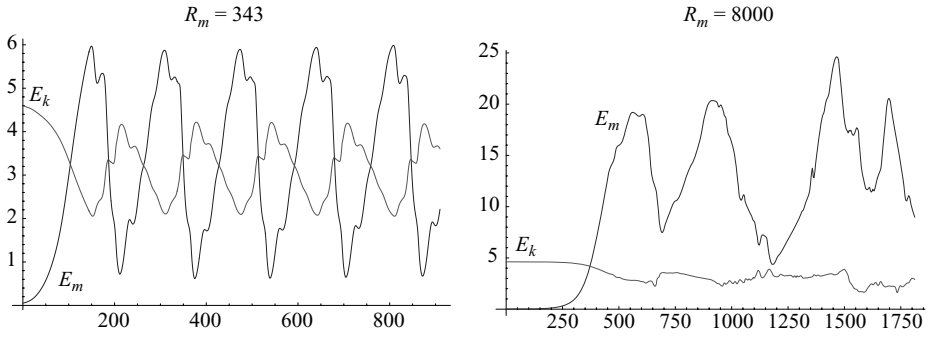


FIGURE 9. E_k and E_m for $R_e = 27$ and $R_m = 343,\ 8000$. High magnetic energy is maintained.

unfortunate, as it suggests that the dynamo mechanism of this configuration will fail for turbulent flows, which are to be expected for real liquid-metal flows.

Even when the steady flow is stable, it is curious that the level of magnetic energy attained is much higher for the more dissipative cases of lower R_e. For $R_e = 27$, for example, a periodic solution occurs at $R_m = 343$ for which E_m sometimes exceeds E_k. This is shown in figure 9 along with the aperiodic case at $R_m = 8000$ for which $E_m > E_k$ always.† Physically, as the magnetic energy grows, the Lorentz force tries to alter the flow into a shape less conducive for dynamo action. At higher R_e this is successful and the growth of E_m is inhibited. At lower R_e, however, viscous forces respond more rapidly to the Lorentz force, re-establishing a flow pattern which generates magnetic energy. The field generation can then be controlled only at high levels of E_m when Ohmic dissipation becomes significant, though still less than the viscous dissipation.

4.1. *A dynamo pump*

The fairly high levels of E_m produced can be used to drive motion down an isolated pipe. If it would also function for the higher values of R_e and turbulent flows obtained in practice, such a hermetically sealed system might be of use in a coolant system of a nuclear reactor, c.f. Plunian, Marty & Alemany (1999). A pressure gradient is applied down only one pipe for $R_e = 27$ and $R_m = 512$. This is found to drive a dynamo in the asymmetric two-pipe system. As the field grows the Lorentz force acts in both pipes, saturating the dynamo action in the first and driving a net flow in the second. For these values the mean flow in the second pipe is found to be about 4% of the flow in the first pipe, and in the same direction. While the laminar flows described in this paper do not apply to real liquid-metal pipe flows, there is no reason why any attainable dynamo should not function as a pump in this manner.

5. Concluding remarks

It has been shown that fully nonlinear, laminar pressure-driven dynamos can exist in the two-pipe configuration for a wide range of magnetic Prandtl numbers. Compared to the single-pipe configuration of Zabielski & Mestel (2006), the two-pipe design is a more powerful dynamo. It shows a greater tendency towards periodic behaviour and is not prone to field reversals. The dynamo energetics differ markedly depending on the relative time scales of eddy turnover, viscous and Ohmic diffusion. At the lower

† Animations of these cases are available with the online version of the paper (animations 2 and 3).

https://doi.org/10.1017/S0022112006004174 Published online by Cambridge University Press

range of R_e the magnetic energy can exceed the kinetic energy, and remains large as R_m increases, even though the dynamo is slow. For higher R_e, the magnetic energy remains smaller than the kinetic. As R_m increases a solution with very low E_m appears at which the dynamo saturates. As R_e increases, the steady flow loses stability, and there are complex interactions between the magnetic and hydrodynamic instabilities. Once the flow becomes seriously unstable, the dynamo action in this configuration is destroyed. For a liquid metal, the physical parameters guarantee that the flow would be turbulent. It is perhaps worth reiterating that the laminar mechanisms studied in this paper do not seem to apply to the turbulent flows obtained in practice (unless one uses a constant 'eddy viscosity'). As Sherlock Holmes observed, the case of a laminar pressure-driven dynamo could be more than a two-pipe problem (Conan-Doyle 1891).

This work was partially supported by EPSRC grant GR/S87539, for which the authors are grateful.

REFERENCES

Benton, E. R. 1979 Kinematic dynamo action with helical symmetry in an unbounded fluid conductor. Part I. *Geophys. Astrophys. Fluid Dyn.* **12**, 313–344.

Berger, S. A., Talbot, L. & Yao, L. S. 1983 Flow in curved pipes. *Annu. Rev. Fluid Mech.* **15**, 461–512.

Conan-Doyle, A. 1891 The red-headed league. *The Strand Magazine* **2(8)**.

Gailitis, A. & Freiberg, Ya. 1977 Theory of a helical MHD dynamo. *Magnetohydrodynamics* **12**, 127–130.

Hall, P. & Horseman, N. J. 1991 The linear inviscid secondary instability of longitudinal vortex structures in boundary layers. *J. Fluid Mech.* **232**, 357–375.

Gilbert, A. D. 2003 Dynamo theory. In *Handbook of Mathematical Fluid Dynamics*, Vol. 2 (ed. S. Friedlander & D. Serre), pp. 355–441. Elsevier.

Lortz, D. 1968 Exact solutions of the hydrodynamic dynamo problem. *Plasma Phys.* **10**, 967–972.

Plunian, F., Marty, P. & Alemany, A. 1999 Kinematic dynamo action in a network of screw motions: application to the core of a fast breeder reactor. *J. Fluid Mech.* **384**, 137–154.

Rädler, K.-H. & Cēbers, A. 2002 The special issue: MHD dynamo experiments. *Magnetohydrodynamics* **38**.

Roberts, P. H. & Soward, A. M. 1992 Dynamo theory. *Annu. Rev. Fluid Mech.* **24**, 459–512.

Zabielski, L. & Mestel, A. J. 1998 Steady flow in a helically symmetric pipe. *J. Fluid Mech.* **370**, 297–320.

Zabielski, L. & Mestel, A. J. 2005 Kinematic dynamo action in a helical pipe. *J. Fluid Mech.* **535**, 347–367.

Zabielski, L. & Mestel, A. J. 2006 Nonlinear dynamos in laminar, helical pipe flow. *Phys. Fluids* **18**, 043602.

https://doi.org/10.1017/S0022112006004174 Published online by Cambridge University Press